PAPER • OPEN ACCESS

Application of STED imaging for chromatin studies

To cite this article: Georgij Kostiuk *et al* 2019 *J. Phys. D: Appl. Phys.* **52** 504003

View the article online for updates and enhancements.

Recent citations

Application of STED imaging for chromatin studies

Georgij Kostiuk[1,2] , **Jonas Bucevičius**[1] , **Rūta Gerasimaitė**[1]
and Gražvydas Lukinavičius[1]

[1] Department of NanoBiophotonics, Max Planck Institute for Biophysical Chemistry, Am Fassberg 11, 37077 Göttingen, Germany
[2] Institute of Biotechnology, Vilnius University, Saulėtekio av. 7, LT- 10257, Vilnius, Lithuania

E-mail: georgij.kostiuk@mpibpc.mpg.de, jonas.bucevicius@mpibpc.mpg.de, ruta.gerasimaite@mpibpc.mpg.de and grazvydas.lukinavicius@mpibpc.mpg.de

Abstract

Chromatin is the information center of a cell. It comprises proteins and nucleic acids that form a highly complex and dynamic structure within the nucleus. Its multiple organization levels span from micrometre to nanometre scale. For many years, the lower levels of chromatin organization have been beyond the resolution limit of fluorescent microscopy, thus impeding research on nucleus architecture, transcription, translation and DNA repair. Recent development in super-resolution fluorescence microscopy enables us to more easily observe objects at the nanometre scale and allows the study of complex cellular structures at unprecedented detail. This review focuses on the application of stimulated emission depletion microscopy for imaging two main components of the chromatin-DNA and the proteins interacting with it.

Keywords: DNA, chromatin, fluorescent labeling, super-resolution microscopy, STED

(Some figures may appear in colour only in the online journal)

1. Introduction

The ability to investigate chromatin organization and dynamics is a key to the understanding of how genetic material is maintained, decoded through transcription and transmitted to daughter cells. Numerous chromatin components have been characterized by classical biochemistry and structural methods, providing invaluable insights on the properties of enzymes and structural proteins, and their interactions with DNA sequences [1]. However, this is insufficient for deciphering molecular mechanisms on the whole cell level, as many crucial functions (such as DNA replication, repair and transcription) are not performed by single proteins or well-defined complexes, but rely on the formation of very large, heterogeneous and dynamic ensembles, involving multiple copies of different proteins and long-range DNA interactions.

In some cases, structural details of such ensembles can be gained by electron microscopy, but dynamics of these processes remain mainly accessible through light microscopy [2]. Fluorescent microscopy is the most flexible method for studying dynamic processes inside the cell, but many chromatin functions are regulated by looping, bending, supercoiling and other conformational changes that occur at length scales below the light diffraction limit of ~250 nm (figure 1). For many years, such structures and processes could only be visualized by indirect methods, such as FRET [3, 4]. This has changed with the introduction of super-resolution fluorescence microscopy techniques that now allow to see the real size of many such structures [5, 6].

There are three major microscopy methods that overcome the light diffraction barrier: stimulated emission depletion (STED) microscopy [7], structured illumination microscopy (SIM) [8] and single molecule localization (SML) microscopy [9, 10]. Each of them has its own advantages, requires different equipment and poses unique requirements on sample preparation and experiment design. These points have been

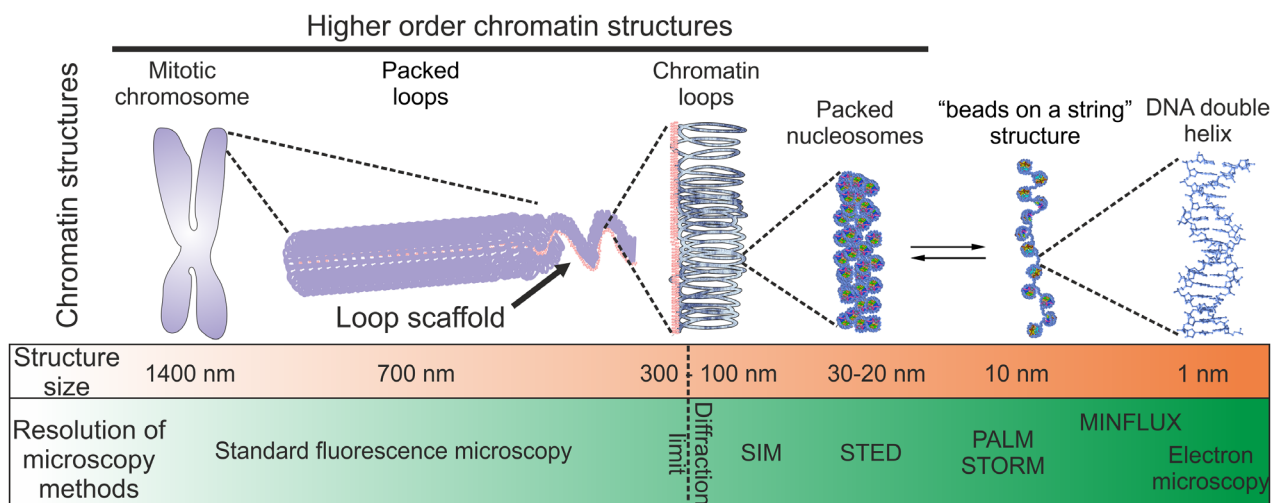J. Phys. D: Appl. Phys. **52** (2019) 504003

G Kostiuk *et al*

Figure 1. Size of structures at different chromatin organization levels in comparison to resolution of different microscopy methods. SIM, structured illumination microscopy; STED, stimulated emission depletion microscopy; PALM, photo-activated localization microscopy; STORM, stochastic optical reconstruction microscopy.

reviewed and the methods have been compared elsewhere [6], and therefore they will not be extensively discussed here. The present review will specifically focus on one of the techniques—STED microscopy—and its impact on chromatin research. In contrast to SIM and SML, imaging by STED microscopy has an inherent advantage of immediately providing a hardware-based image with improved resolution without the need for post-processing procedures, which makes it less prone to incorrect data processing and interpretation. With the example of STED microscopy, we will discuss how the super-resolution imaging is transforming chromatin research. We will begin by describing the fluorescent dyes that are used for labeling DNA and chromatin components. Then we will provide illustrative examples, where improved resolution offered by STED microscopy was instrumental to obtain fundamentally novel information or explain previously elusive phenomena.

2. Fluorophores used in STED microscopy

Chromatin components can be visualized in different ways: total DNA can be stained with sequence unspecific dyes, specific DNA sequences can be hybridized with fluorescently labeled complementary probes; chromatin proteins can be visualized with fluorescently labeled antibodies or as fusions with fluorescent proteins. STED microscopy poses relatively few specific requirements on a fluorophore itself: it must be photostable in order to withstand much higher laser powers than during conventional confocal imaging, and it must show efficient stimulated emission with minimal re-excitation at the wavelength of the depletion laser. The overview of fluorophores used for chromatin imaging by STED is provided in table 1. There are no strict rules to predict compatibility of the dye with STED microscopy. The most often used STED-compatible fluorophores are derivatives of rhodamines. In contrast, cyanines show limited STED-compatibility, providing little gain in resolution, with the exception for DNA intercalating dyes based on cyanine scaffold (see below).

Autofluorescent proteins can also be used for STED imaging, but their lower photostability compared to the organic dyes results in less acquired frames [11]. When considering fluorescent protein tags, the proteins operating at red or far-red spectral region should be the first choice, as imaging at these wavelengths induces the least phototoxicity [12–14].

In contrast to fluorescent proteins, interaction of organic dyes with DNA is fluorogenic – usually, DNA-specific dyes are non-fluorescent or weakly fluorescent when free in solution and their fluorescence dramatically increases after reversible binding to DNA. This enhances the contrast of the images and reduces bleaching via fluorophore exchange with a pool of dye present in the medium [15].

Other requirements for small molecule fluorescent probes used for STED imaging are the same as in conventional imaging techniques: good solubility in aqueous solutions, sequence or structure specificity, high binding affinity and, ideally, turn-on fluorescence upon target binding. In case of living cell imaging, low toxicity, good cell permeability and low off-targeting are essential.

3. DNA imaging

3.1. In vitro DNA imaging

Fluorescent probes targeting DNA have become indispensable tools in cell biology, molecular biology, chemical biology and drug discovery fields. Taking into account the increasing number of new fluorescent probes developed each year, the availability of fluorescent DNA stains is also steadily increasing [16, 17].

First successful STED imaging of DNA *in vitro* was demonstrated by Persson *et al* [18] by employing the standard DNA bis-intercalating dye **YOYO-1** (figure 2(a) and figure 3(a)), which belongs to dimeric cyanine class of dyes. **YOYO-1** shows a 500-fold fluorescence enhancement upon binding to DNA. The authors demonstrated a six fold improvement in resolution over standard confocal microscopy by exciting

J. Phys. D: Appl. Phys. **52** (2019) 504003

G Kostiuk *et al*

Table 1. STED microscopy compatible fluorophores used to label chromatin components.

Fluorophore name	λ_{max}^{abs} (nm)	ε_{max}^{abs} (M^{-1} cm^{-1})	λ_{max}^{em} (nm)	QY	Depletion laser (nm)	References
Dyes directly interacting with DNA						
YOYO-1	491	98 900	508	0.52	568	[18, 19]
5-580CP-Hoechst	588	84 200	613	0.37	775	[17]
5-610CP-Hoechst	614	84 300	641	0.43	775	[17]
5-GeR-Hoechst	641	26 600	660	0.39	775	[17]
5-SiR-Hoechst	651	38 000	672	0.37	775	[17]
6-SiR-Hoechst	654	54 600	677	0.16	775	[17, 24]
JF$_{646}$-Hoechst	664	NR[c]	673	NR[c]	775	[15]
Ru-NLS[a]	454	NR[c]	617	NR[c]	660	[29]
LC[b]	468	129 900	555	0.0031	595	[30]
STED-compatible dyes used in the chromatin studies						
Aberrior STAR440SXP	432	33 000	511	0.57	592	[38, 41]
Alexa Fluor 488	495	73 000	519	0.92	590	[44, 36, 46]
Oregon Green488	498	85 000	526	0.91	592	[45, 49]
Chromeo 505	514	70 000	530	0.30	592	[38, 41]
Cy3B	559	130 000	573	0.67	NR	[50]
Aberrior STAR 580	587	85 000	607	0.90	775	[43]
Alexa Fluor 594	590	92 000	617	0.66	775	[46]
Aberrior STAR 635P	638	120 000	651	0.90	775	[43]
Atto 647N	646	150 000	664	0.65	750 or 775	[31, 35, 51]
SiR	645	100 000	670	0.40	775	[36]

Note: spectral properties obtained from the web site of the corresponding manufacturer: www.abberior.com/, www.thermofisher.com/, www.atto-tec.com/ or www.activemotif.com/. [a]Ru-NLS in acetonitrile (properties of free dye). [b]LC in DMSO:H2O 1:1 (Properties of free dye). [c]Not reported.
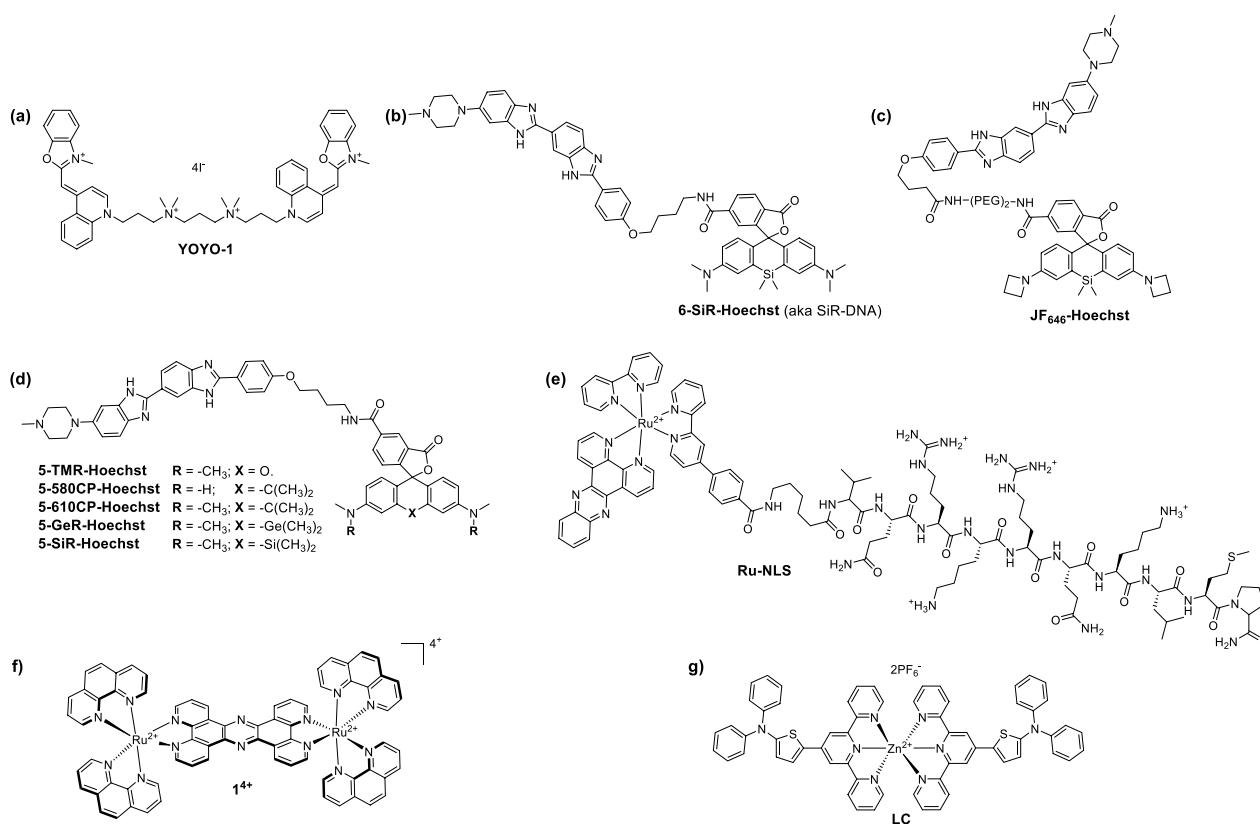
Figure 2. Molecular structures of fluorescent DNA dyes compatible with STED microscopy.
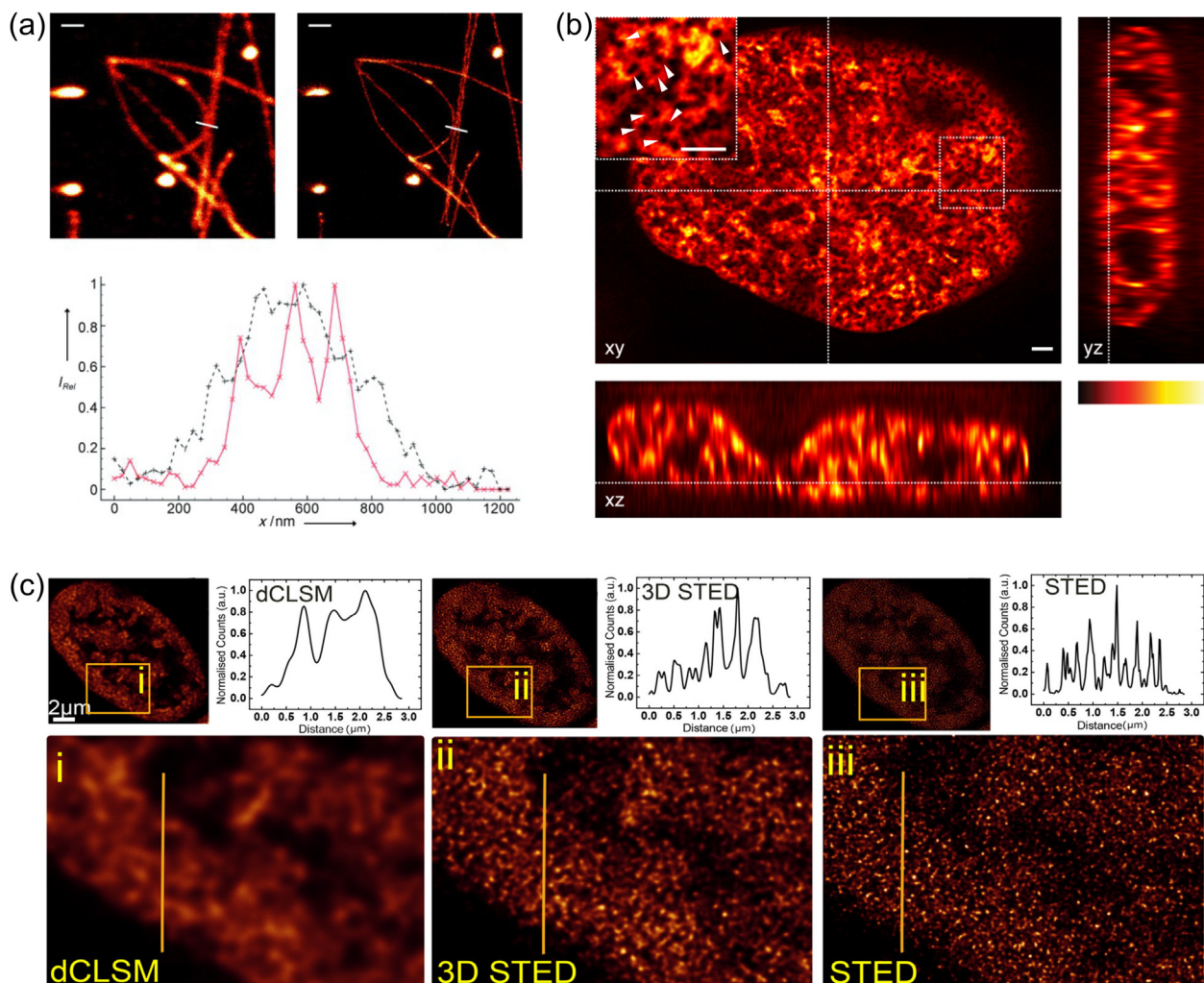
Figure 3. Examples of confocal and STED images of DNA directly labeled with fluorophores. (a) Confocal and STED images of **YOYO-1** stained λ DNA (basepair:dye = 5:1). Scale bars: 1 μm. Below, the line profiles from the STED (solid red line) and confocal (dotted black line) along the white lines in the images. Adapted from [18] John Wiley & Sons. [Copyright © 2011 WILEY-VCH Verlag GmbH & Co. KGaA, Weinheim]. (b) *xy*, *xz* and *yz* planes of a deconvolved STED *z*-stack of a living HeLa cell stained with 1 μM 5-SiR-Hoechst in DMEM growth medium. Arrows indicate heterochromatin exclusion zones. Scale bars: 1 μm in the large image and 0.5 μm in the inset. Reprinted with permission from [27]. Copyright (2019) American Chemical Society. (c) Live cells stained with 500 μM **1^{4+}** and imaged by: HyVolution-confocal imaging combined with deconvolution algorithm (dCLSM), 3D-STED, and STED. Panels (i)–(iii) show magnified images at positions marked by boxes. Fluorescence intensity profiles are generated from the lines shown in (i)–(iii). Reprinted with permission from [28]. Copyright (2017) American Chemical Society.

the dye at 470 nm and using 568 nm emission depletion laser. The increased resolution allowed to resolve the occurrence of bends and kinks along phage λ DNA. The kinks were attributed to the sequence specific binding of the **YOYO-1** dye and to the binding of proteins or other small molecules. Moreover, it was demonstrated that a four-fold improvement of resolution over confocal imaging could be achieved by using a 647 nm depletion laser where the **YOYO-1** emission is just 3% of its maxima, thus demonstrating that the depletion laser can be applied over a wide wavelength range.

YOYO-1 was also used for the accurate determination of fragment lengths produced by digesting λ DNA with the restriction enzymes R.*Bst*EII or R.*Hind*III. For linear DNA measurement, DNA fragments can be stretched by capillary force, force flow or dynamic molecular combing (DMC). Kim *et al* has combined DMC with STED microscopy, due to its simplicity and superb reproducibility [19]. Immersing

silanized coverslip in a Teflon chamber with DNA fragments followed by pulling at a constant speed of 200 μm s^{-1} ensured binding of one DNA end to a coverslip and rupture-free DNA stretching. Subsequent continuous-wave STED imaging led to the determination of fragment lengths ranging from 117 to 23 130 bp. Importantly, fragments of similar lengths, such as 117 and 224 bp or 1264 and 1371 bp, could be distinguished. The authors proposed that the measurement precision is sufficient for their method to have potential for the diagnosis of the genetic disorders caused by copy number variation, such as trinucleotide repeat disorder [19].

3.2. In vivo DNA imaging

Traditionally, dyes excited by UV light (DAPI and Hoechst), have been used for staining DNA in the nucleus of living and fixed cells [20, 21]. These dyes are not suitable for

super-resolution microscopy and imaging by blue light results in significant phototoxicity [22, 23]. In 2015, Lukinavičius *et al* introduced a far-red DNA stain **6-SiR-Hoechst** (figure 2(b)) (aka SiR-DNA) [24] for live-cell imaging. The probe was designed by modular Hoechst tagging strategy [25] and consists of STED compatible far-red dye 6-carboxyl silicon-rhodamine [26] conjugated to Hoechst as DNA binding moiety by a short aliphatic linker [17]. **6-SiR-Hoechst** is a highly-photostable, fluorogenic dye showing approximately 50-fold fluorescence increase upon binding to DNA and its fluorescence can be efficiently switched OFF by 775 nm STED laser. The proposed mechanism of fluorogenicity is different from the parent Hoechst 33342, and at least partially results from a shift of the equilibrium of silicon-rhodamine from the non-fluorescent spirolactone to the fluorescent zwitterion form. The relationship between probe structure and properties was further investigated in a recent study by Bucevičius *et al* which demonstrated that a minimal change in the attachment point of the dye has a dramatic effect on the properties of the final probe [27]. Specifically, it was revealed that 6-carboxylrhodamine dye containing probes, such as **6-SiR-Hoechst**, exhibit dual-mode binding to DNA and form a dimmer complex at high DNA concentrations, whilst 5-carboxylrhodamine dye containing probes exclusively exhibit single-mode binding to DNA, which results in lower cytotoxicity and up to 10-fold brighter nuclear staining. This feature was demonstrated with tetramethylrhodamine (**5-TMR-Hoechst**), two carbopyronines (**5-580CP-Hoechst** and **5-610CP-Hoechst**), silicon-rhodamine (**5-SiR-Hoechst**) and germanium-rhodamine (**5-GeR-Hoechst**) (figures 2(d) and 3(b)). Employing these highly efficient probes allowed to estimate the heterochromatin exclusion zones (~165 nm) in nuclear pore region in living cells and intact chicken erythrocytes. Moreover, a wide colour selection of probes allowed two colour STED imaging of intact nucleated erythrocytes – a system where imaging is highly complicated by the haemoglobin absorption.

Another infrared DNA probe of similar design, **JF646-Hoechst** (figure 2(c)), consisting of JF646 fluorophore conjugated to Hoechst by a C4-PEG2 linker, allowed visualization of small DNA loops in the mitotic chromosomes of fixed HeLa cells by STED microscopy [15].

In 2016, Byrne *et al* used ruthenium (II) metal complex luminophore as a fluorescent DNA probe for STED microscopy [29]. Transition metal complex luminophores, such as Ru (II) polypyridyl complexes, bear a number of useful properties for fluorescence microscopy: large Stokes shift, long lived emissive states usually arising from phosphorescent emission and good photostability. However, the inability to cross membranes has hampered the use of metal-organic complexes for super-resolution imaging of living cells earlier. Byrne *et al* have overcome this issue by conjugating Ru(II) polypyridyl complexes to cell penetrating peptides such as nuclear localisation sequences (NLS). In particular, previously known DNA binding metal complex [Ru(dppz)(bpy)(bpyArCOOH)]$^{2+}$ was conjugated to NLS (VQRKRQKLMP) of the transcription factor NF-κB by peptide coupling to yield **Ru-NLS** probe (figure 2(e)). The emission of this complex switches OFF in water, but it starts to emit strongly upon

binding to DNA due to the presence of the phenazine ligand. The stained nuclei of living HeLa cells were imaged by excitation at 488 nm and STED laser at 660 nm, which overlaps with the broad ruthenium ^{3}MLCT emission band at 611 nm. The turn-on property of the probe combined with excellent STED performance allowed the authors to identify cell cycle phases through a series of STED images of a labeled HeLa cell. Moreover, it was demonstrated that long lived phosphorescent emission makes these probes particularly amenable for time-gated STED applications. Time-gating the detection in STED microscopy serves as a spatial filter, reducing background signal and the point-spread function of the interrogation volume to improve image resolution. A time delay is introduced after the excitation to maximize the number of fluorophores in the depletion donut that are switched-off. Moreover, it is also a very useful approach in resolving two dyes with different excited state lifetimes even if the dyes emit light of similar wavelengths. Inspired by these results, Sreedharan *et al* successfully applied a dinuclear Ru (II)-based complex **1**$^{4+}$ (figure 2(f) and figure 3(c)) in STED microscopy [28]. Surprisingly, no cell penetrating peptides were needed as the probe was cell permeable. The complex also demonstrated fluorescence turn-ON upon DNA binding. Moreover, a selective staining of mitochondria or nucleus could be obtained by adjusting the concentration of the complex-concentrations below 5 μM stained mitochondria and at concentrations above 18 μM, mitochondrial emission was not discerned due to the more intense emission of complex bound to nuclear DNA. The biggest advantage of this STED compatible DNA probe is that it can be easily synthesised on a gram scale and no conjugation to targeting moieties is required. Because of its high photostability, this complex is compatible with 3D-STED imaging, and provides high resolution along all three axes (figure 3(c)).

Recently, a thiophene based Zn(II) complex **LC** (figure 2(g)), which can specifically target live cell mitochondrial DNA by intercalation, has been described [30]. The fluorescence of this probe turns-on upon DNA binding and it is excited by 405 nm (one photon absorption) or 840 nm (two photon absorption) and is compatible with 595 nm STED laser. The authors reported that this probe exhibits low cytotoxicity at low micromolar concentration range over a period of 24 h. STED imaging revealed ultra-detailed structures corresponding to mtDNA distributed within mitochondrial inner matrix with an approximate 40–70 nm separation between two stripes. Moreover, the authors claim that the photophysical properties of the LC probe can be tuned by changing a bridging unit—thiophene—and by attaching different electron-donors, thus resulting in a tuneable platform for the design of promising bioimaging probes for super-resolution imaging.

4. Imaging of proteins interacting with DNA

Proteins interacting with DNA are particularly interesting objects because these complexes play a central role in gene regulation, repair and packing. Heller *et al* resolved single proteins interacting with DNA at high concentration
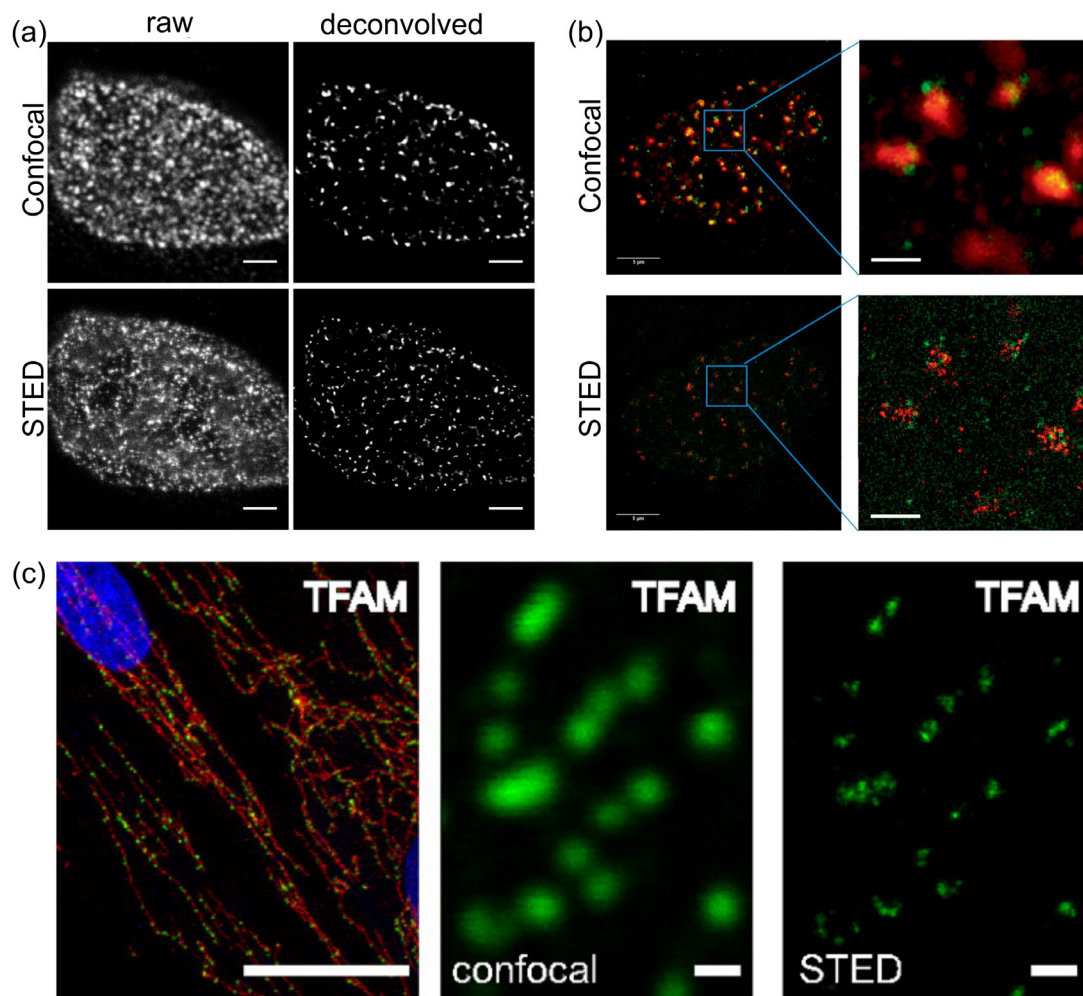
Figure 4. Examples of confocal and STED images of proteins interacting with DNA labeled with antibody-fluorophore conjugates. (a) A series of *Z* slices obtained from MRC5 cells labeled for PCNA in confocal and STED modes. The raw images were restored using the Huygens (SVI) software for deconvolution. Scale bars: 2 μm. Reproduced from [35]. CC BY 4.0. (b) Confocal and STED overlay images of fixed HeLa cells labeled with primary antibody to γ-H2AX and 53BP1 followed by fluorescently tagged secondary antibody with Alexa Fluor 488 and SiR, respectively. Scale bars: 5 μm in large images and 1 μm in the zoom-in images. Reproduced with permission from [36]. [© 2019 Radiation Research Society]. (c) TFAM (green, anti-TFAM antibody) is located in nucleoids in the mitochondrial network (red, anti-TOM20 antibody) of human fibroblasts. Nuclear DAPI-staining in blue. Scale bar 20 μm. Two panels on the right show zoomed-in confocal and STED images of the nucleoids. Scale bar 0.5 μm. Reproduced with permission from [37].

using a setup comprised of: (1) optical tweezers for DNA conformation and tension control, (2) beam-scanning confocal fluorescence microscope for protein imaging on the stretched DNA and (3) 1D STED nanoscopy to distinguish individual labeled proteins at high protein density on DNA. The experiments were performed on λ DNA fused to 2 polystyrene spheres stretched with optical tweezers. Full width at half maximum (FWHM) of 50 nm was obtained when imaging Atto 647N labeled restriction enzymes EcoRV and BsoBI bound to stretched DNA. The experiments revealed that at least 5 pN stretching force was required to obtain effective resolution. The combined setup was also used for investigating DNA-binding dynamics of human mitochondrial transcription factor (TFAM) labeled with Atto 647N. Time traces of single TFAM molecules at high protein concentrations were resolved and mean diffusion constant $D = 0.028$ μm^2 s^{-1} was determined, which is much

slower than that measured for monomeric TFAM ($D = 0.08$ μm^2 s^{-1}), probably due to oligomerisation [31].

Similar to small molecule DNA binders, histones can be used for visualizing overall chromatin structure [32]. Imaging cells stained with antibody against core histone H3 has revealed chromatin domains of 40–70 nm size in neonatal rat ventricular myocytes, primary neurons, HeLa and HEK293 cell lines. The authors proposed that improved resolution allows tracking individual chromatin fibers, which provides an overview of the global chromatin structure and facilitates distinguishing between chromatin and interchromatin regions. Treatment of cells with hypertrophic agonist isoproterenol resulted in redistribution of staining intensities, which was interpreted as global chromatin rearrangements. Although interesting, such data lacks the information on the identity of the genomic regions undergoing change, which precludes mechanistic interpretations.

J. Phys. D: Appl. Phys. **52** (2019) 504003

G Kostiuk *et al*

More specificity can be achieved by staining one or several chromatin components (proteins and/or DNA sequences) that are involved in a particular process. For example, visualization of centromeric and pericentromeric satellite repeats by FISH (fluorescence *in situ* hybridization) has revealed massive distension of these, otherwise tightly packed DNA regions, early at the onset of cell senescence [33]. These changes were of a massive enough scale (up to 5 μm) to be detected by conventional confocal microscopy. However, STED microscopy provided finer details on their structure: in both, proliferating and senescent cells, peri/centromeric satellite DNA comprises globular domains linked by DNA threads [34]. In proliferating cells, however, these globules are held in close proximity, while in senescent cells the threads are much more extended, suggesting loss of a factor that originally holds them together. This information offers a way to further address the mechanisms underlying these changes.

Research fields dealing with such complex processes as DNA replication, repair and recombination have greatly benefitted from the super-resolution co-localization techniques for investigation of heterogeneous ensembles that span kilobases of DNA and involve multiple copies of chromatin proteins (reviewed in [38, 39]). In many cases, improved resolution allows to observe the real dimensions of the structures of interest, although in each case this must be carefully verified by comparing the obtained dimensions with those determined by either electron microscopy or other independent methods.

DNA replication in mammalian cells occurs in discrete subnuclear locations—replication foci or factories. These factories are sized below diffraction limit (<250 nm), assemble during S phase and contain high local concentrations of replication enzymes. Green *et al* was the first group that analyzed DNA replication using STED microscopy [35]. They stained PCNA (proliferating cell nuclear antigen) and RPA (replication protein A) with antibodies. STED microscopy images revealed that replication factories are approximately 150 nm in diameter, and up to 1400 of replication foci, each containing 2–3 replication forks, exist in an early S-phase nucleus (figure 4(a)). These numbers are up to 10-fold different compared to the numbers obtained by confocal microscopy highlighting the importance of super-resolution imaging. Furthermore, the replication factory size is close to the dimensions obtained by electron microscopy demonstrating the reliability of the performed measurements. Taking advantage of the increased resolution, the authors noticed ~40% reduction in number and ~30% increase in diameter of replication factories in the cells treated with the replication inhibitor hydroxyurea. Such subtle changes cannot be reliably identified by standard confocal imaging.

DNA is under constant assault by various internal and external agents which can lead to heterocyclic base, sugar or phosphodiester damage. The latter can result in difficult to repair and potentially deadly double-strand breaks. Many studies have employed STED microscopy to study DNA double-strand break repair. Histone H2AX phosphorylation on serine residue 139, known as γ-H2AX, is a common marker of double-strand breaks, which is often used to estimate the extent of DNA damage [40].

A recent study used STED microscopy to examine organization of nucleoprotein complexes inside the ionizing radiation-induced foci (IRIF), which encompass mega-base pair chromatin regions, containing phosphorylated histone γ-H2AX and multiple DNA repair and DNA damage signaling factors [41]. Both, the mediator protein 53BP1 that is involved in the non-homologous end joining and Rad51 protein that links complementary chromatin strands in homologous recombination, belong to this compartment. Although γ-H2AX and 53BP1 co-localize on a micrometer scale in confocal images, imaging with STED showed nearly complete anti-correlation of the two signals (figure 4(b)). An earlier study has similarly shown anti-correlation between 53BP1 and Rad51 signals [42]. This allowed building IRIF model, where each of these proteins occupy different positions in accordance to their distinct functions in DNA repair: 53BP1 occupies perichromatin region, but does not penetrate the dense chromatin domains marked by γ-H2AX, while Rad51 locates at the center, in the single-stranded DNA compartment. Such arrangement is consistent with the known role of Rad51 in the resection of DNA ends, while 53BP1 in the periphery may serve to limit the resection and stabilize the whole structure.

Another study investigated the structure of DSB repair sites by integrating the data from super-resolution microscopy and whole-genome sequencing [38]. This study has found that γ-H2AX foci that are identified by conventional microscopy upon x-ray irradiation, in reality represent higher order chromatin structures of discontinuously phosphorylated chromatin, that consist of clustered γ-H2AX nano-foci of 40–160 kbp and ~200 nm in size. Each of such clusters was found to contain one DSB and distribution of these γ-H2AX clusters changed according to the progression of repair. Majority of data presented in this paper was produced with 3D-SIM microscopy, and imaging with STED, that provided a further 2-fold improvement in resolution, was mainly used to verify the findings.

Immunostaining of γ-H2AX and DNA repair protein 53BP1 was used to compare pseudo and real super-resolution techniques: Zeiss Airyscan and Leica HyVolution 2, STED, ground-state depletion microscopy followed by individual molecule return (GSDIM) and structured illumination microscopy (SIM) [36]. In agreement with previous studies, the authors found that all techniques showed much improvement in the spatial resolution significantly below diffraction limit, ranging from 40 to 140 nm. Super-resolution imaging increased precision of DNA repair foci localization but this did not always lead to identification of a higher number of foci. In addition, the authors expressed another DNA repair protein Ku80 as GFP-fusion and found that γ-H2AX, 53BP1 and Ku70/80 repair proteins do not fully co-localize in the higher order chromatin structure.

Dual-Immuno FISH was used to co-localize telomeric DNA sequences, γ-H2AX and 53BP1 to follow the appearance and structure of telomere-associated foci in mice and human cardiomyocites upon aging [43]. This study addressed the role of irreparable telomere damage and cellular senescence in age-related cardiac dysfunction. The high resolution of STED allowed better discrimination of telomere lengths, and enabled to resolve individual telomeres in telomere clusters.
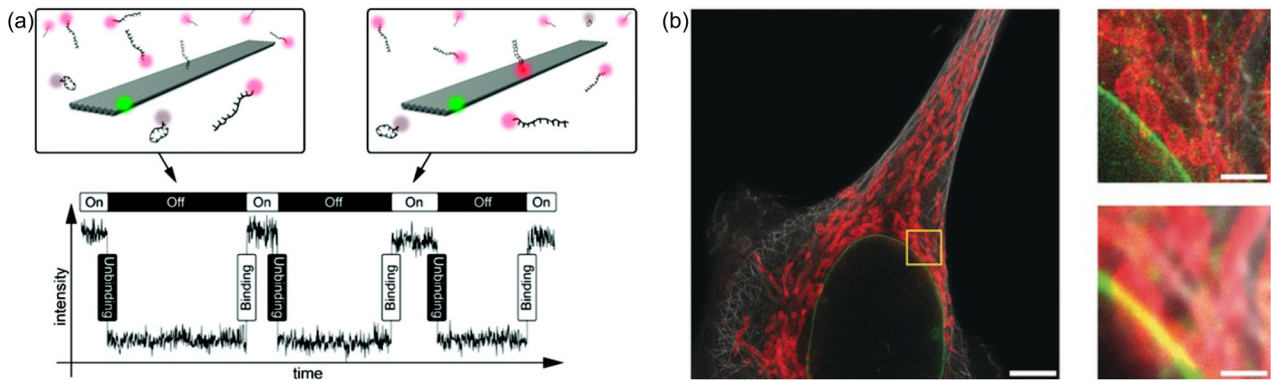
J. Phys. D: Appl. Phys. **52** (2019) 504003

G Kostiuk *et al*

Figure 5. The principle of DNA-PAINT labeling and an example image obtained with Exchange-STED. (a) DNA-PAINT relies on the DNA hybridization. A structure of interest is labeled with a short DNA, a so-called 'docking' strand, while a fluorescent label is conjugated to a complementary 'imager' strand. Fast diffusing labeled imager strands in solution are invisible in the absence of binding to the docking strand. This resembles the fluorescence OFF-state. Upon hybridization of the imager strands with the docking strand, fluorescent label is immobilized on the structure-of-interest and its fluorescence can be registered and localized by different microscopy techniques. Transient nature of the interaction between docking and imager strands allows registering multiple binding events, thus resembling blinking of a fluorophore. Many variations of this basic principle are being developed, mainly aiming at increasing multiplexing and improving signal-to-noise ratio [54]. Reprinted with permission from [53]. Copyright (2010) American Chemical Society. (b) Overlay image of the three-round Exchange-STED *in situ* α-tubulin is imaged in round 1, lamin B in round 2 and TOM20 in round 3. Zoom-in of the highlighted area corresponding to diffraction-limited representation (bottom) and increased spatial resolution in STED (top). Scale bars: 5 μm (large image), 1 μm (zoom-in). [51] John Wiley & Sons. [© 2017 Wiley-VCH Verlag GmbH & Co. KGaA, Weinheim].

This provided the evidence that length-independent telomere damage, rather than telomere shortening, underlies the induction of senescence in the post-mitotic cardiomyocytes.

Another study used STED microscopy for investigating double strand break repair by RecA-catalyzed homologous recombination in bacteria [44]. It found that damage induced RecA foci are typically between 50 and 200 nm in length. The authors have developed a new method for detecting RecA complexes in the nucleoids spread on a glass surface, and stained with anti-RecA and anti-SSB antibodies. They have demonstrated that RecA-K250N, a loss-of-function ATPase-defective mutant, spontaneously form DNA-bound complexes, which cause cytotoxicity. Furthermore, using combination of super-resolution microscopy and biochemistry, they could prove that ATPase activity of RecA prevents accumulation of toxic complexes (foci) caused by binding of RecA to undamaged regions of dsDNA.

STED microscopy was used to dissect a new role of condensin in the maintenance of sister chromatids cohesion during meiosis [45]. In this case, high imaging resolution was essential to demonstrate that the reduced levels of cohesin in condensin I mutants interfere with the recruitment of synaptonemal complex central region proteins. Importantly, in the case of conventional fluorescence microscopy, the proteins under study appear to co-localize, thus making it impossible to resolve the mutant phenotype.

Viral infections are followed by the replication of the viral genome. Recently, STED microscopy was applied to track DNA during lytic cycle of herpes simplex virus 1 infections [46]. The authors used immunofluorescence and FISH to observe positions of DNA, viral single strand binding protein ICP8 and host RNA polymerase II. They found that regions of DNA replication marked by ICP8 are spatially separated from regions of active transcription. In addition, they noted that the viral genome is expanding spatially during the replication

process. Again, the use of STED microscopy considerably increased the precision of these observations.

Mitochondrial DNA encodes genes required for oxidative phosphorylation, rRNAs and tRNAs. mtDNA is packaged in a compact structure called nucleoid, which is composed of DNA-protein complexes. Kukat *et al* conducted an interesting study in which STED imaging revealed that mitochondrial nucleoids in a variety of mammalian species had a mean diameter below $\sim$100 nm, which was much smaller than anticipated (figure 4(c)) [37]. The authors have used antibodies against DNA, mitochondrial transcription factor A (TFAM), or incorporated BrdU. A later study that focused on TFAM showed that mtDNA packing is a multistep process initiated by TFAM aggregation, cross-strand binding and DNA looping [47]. It was demonstrated that increased mtDNA copy number results from the increased nucleoid number, but not the change in their sizes. The authors suggested that a fundamental organizational unit of mitochondrial nucleoid is a single copy of mtDNA packed by TFAM. Importantly, all these observations were backed-up by electron microscopy. However, even such detailed studies do not provide a complete picture of mitochondrial nucleoid organisation. Stochastic 3D super-resolution microscopy methods consistently provide wider nucleoid size distributions than those obtained by STED and suggest existence of nucleoid clusters and/or larger nucleoids of irregular shape. This discrepancy can only be resolved by imaging the same samples with different techniques in parallel (reviewed in [48]).

5. Points accumulation for imaging in nanoscale topography (PAINT) imaging

All types of microscopy benefit from a high number of photons arriving from the structure under investigation. This stimulates the development of brighter and more photostable

J. Phys. D: Appl. Phys. **52** (2019) 504003

G Kostiuk *et al*

dyes. An alternative strategy involves exchanging fluorophores after photobleaching during the image acquisition. For the first time, such method was applied for SML microscopy and called Point Accumulation for Imaging Nanoscale Topography (PAINT) [52]. The versatility of DNA makes it an ideal PAINT probe. In particular, DNA is used as a fluorophore carrier and affinity tag for staining structures-of-interest based on interactions between two complementary DNA strands. This has led to development of a whole family of imaging methods—DNA PAINT (figure 5(a)) [53, 54].

DNA PAINT principle was employed for visualization of multiple objects by the method called DNA exchange imaging (DEI). It uses DNA-barcoded antibodies (typically 9–10 nucleotides) against multiple targets that are detected by sequential application and gentle removing of the corresponding complementary DNA strands, labeled with the same fluorophore. This works in combination with different imaging platforms: Exchange Confocal, Exchange-SIM, Exchange-STED and Exchange-PAINT. Exchange-STED was applied for imaging four proteins (GFAP, pNFH, SynapsinI and Bassoon) in fixed DIV14 mouse hippocampal neurons. Localizations of target protein were determined by sequential exchange of corresponding imager strands linked to one fluorophore—Cy3B [50]. To reduce the background, the imaging strands were labeled with fluorophores at both ends and the fluorescence of the unbound imager strands was quenched due to high local fluorophore concentration [49].

A different approach was applied for imaging DNA origami, where stable imager strand binding and low background was achieved by using longer complementary DNA and including denaturing agent in the washing buffer. A library of six-helix-bundle DNA structures carrying four specific single stranded DNA extensions arranged in four spots approximately 113 nm apart was investigated. Sequential labeling and imaging cycles resolved the labeled positions and deciphered unique barcodes on the origami structure. The specific labeled positions in the barcode were detected with 91% accuracy. This technique was also applied for cellular proteins. The combination of DNA barcoded antibody imaging resulted in excellent quality multicolor STED images (figure 5(b)) [51].

6. Conclusions and future perspectives

We have highlighted the most prominent examples of application of STED microscopy for the imaging of DNA and DNA-interacting proteins. These studies clearly demonstrate the benefits of super-resolution imaging to uncovering the important details of chromatin structure and function. Most of the work presented here was performed on fixed cells, but as the imaging speed increases and the labeling methods get optimized, undoubtedly there will be more studies addressing the dynamic processes in living cells. The ongoing further developments towards increased resolution and imaging speed will be able to provide even more detailed picture. For example, the recently introduced MINFLUX imaging method achieves

resolutions close to 1 nm and has been already applied for imaging DNA origami and tracking ribosomes in living cells [55, 56]. This method has a great potential to advance our understanding of basic chromatin biology and facilitate the development of novel therapies.

ORCID iDs

Georgij Kostiuk https://orcid.org/0000-0003-1059-9419
Jonas Bucevičius https://orcid.org/0000-0001-5725-8940
Rūta Gerasimaitė https://orcid.org/0000-0003-4898-1496
Gražvydas Lukinavičius https://orcid.org/0000-0002-7176-1793

References

[1] Kouzarides T 2007 Chromatin modifications and their function *Cell* **128** 693–705
[2] Wilson M D and Costa A 2017 Cryo-electron microscopy of chromatin biology *Acta Crystallogr.* D **73** 541–8
[3] Lou J, Scipioni L, Wright B K, Bartolec T K, Zhang J, Masamsetti V P, Gaus K, Gratton E, Cesare A J and Hinde E 2019 Phasor histone FLIM-FRET microscopy quantifies spatiotemporal rearrangement of chromatin architecture during the DNA damage response *Proc. Natl Acad. Sci. USA* **116** 7323–32
[4] Nakaoka S, Sasaki K, Ito A, Nakao Y and Yoshida M 2016 A genetically encoded FRET probe to detect intranucleosomal histone H3K9 or H3K14 acetylation using BRD4, a BET family member *ACS Chem. Biol.* **11** 729–33
[5] Flors C 2013 Super-resolution fluorescence imaging of directly labelled DNA: from microscopy standards to living cells *J. Microsc.* **251** 1–4
[6] Sahl S J, Hell S W and Jakobs S 2017 Fluorescence nanoscopy in cell biology *Nat. Rev. Mol. Cell Biol.* **18** 685–701
[7] Hell S W and Wichmann J 1994 Breaking the diffraction resolution limit by stimulated emission: stimulated-emission-depletion fluorescence microscopy *Opt. Lett.* **19** 780–2
[8] Gustafsson M G 2005 Nonlinear structured-illumination microscopy: wide-field fluorescence imaging with theoretically unlimited resolution *Proc. Natl Acad. Sci. USA* **102** 13081–6
[9] Moerner W E and Kador L 1989 Optical detection and spectroscopy of single molecules in a solid *Phys. Rev. Lett.* **62** 2535–8
[10] Betzig E 1995 Proposed method for molecular optical imaging *Opt. Lett.* **20** 237–9
[11] Wang L, Frei M S, Salim A and Johnsson K 2019 Small-molecule fluorescent probes for live-cell super-resolution microscopy *J. Am. Chem. Soc.* **141** 2770–81

[12] Kamper M, Ta H, Jensen N A, Hell S W and Jakobs S 2018 Near-infrared STED nanoscopy with an engineered bacterial phytochrome *Nat. Commun.* **9** 4762

[13] Hense A, Prunsche B, Gao P, Ishitsuka Y, Nienhaus K and Nienhaus G U 2015 Monomeric Garnet, a far-red fluorescent protein for live-cell STED imaging *Sci. Rep.* **5** 18006

[14] Waldchen S, Lehmann J, Klein T, van de Linde S and Sauer M 2015 Light-induced cell damage in live-cell super-resolution microscopy *Sci. Rep.* **5** 15348

[15] Spahn C, Grimm J B, Lavis L D, Lampe M and Heilemann M 2019 Whole-cell, 3D, and multicolor STED imaging with exchangeable fluorophores *Nano Lett.* **19** 500–5

[16] Suseela Y V, Narayanaswamy N, Pratihar S and Govindaraju T 2018 Far-red fluorescent probes for canonical and non-canonical nucleic acid structures: current progress and future implications *Chem. Soc. Rev.* **47** 1098–131

[17] Bucevičius J, Lukinavičius G and Gerasimaitė R 2018 The use of hoechst dyes for DNA staining and beyond *Chemosensors* **6** 18

[18] Persson F, Bingen P, Staudt T, Engelhardt J, Tegenfeldt J O and Hell S W 2011 Fluorescence nanoscopy of single DNA molecules by using stimulated emission depletion (STED) *Angew. Chem., Int. Ed. Engl.* **50** 5581–3

[19] Kim N, Kim H J, Kim Y, Min K S and Kim S K 2016 Direct and precise length measurement of single, stretched DNA fragments by dynamic molecular combing and STED nanoscopy *Anal. Bioanal. Chem.* **408** 6453–9

[20] Kapuscinski J 1995 DAPI: a DNA-specific fluorescent probe *Biotech Histochem.* **70** 220–33

[21] Latt S A, Stetten G, Juergens L A, Willard H F and Scher C D 1975 Recent developments in the detection of deoxyribonucleic acid synthesis by 33258 Hoechst fluorescence *J. Histochem. Cytochem.* **23** 493–505

[22] Coutu D L and Schroeder T 2013 Probing cellular processes by long-term live imaging—historic problems and current solutions *J. Cell Sci.* **126** 3805–15

[23] Purschke M, Rubio N, Held K D and Redmond R W 2010 Phototoxicity of Hoechst 33342 in time-lapse fluorescence microscopy *Photochem. Photobiol. Sci.* **9** 1634–9

[24] Lukinavičius G *et al* 2015 SiR-Hoechst is a far-red DNA stain for live-cell nanoscopy *Nat. Commun.* **6** 8497

[25] Nakamura A, Takigawa K, Kurishita Y, Kuwata K, Ishida M, Shimoda Y, Hamachi I and Tsukiji S 2014 Hoechst tagging: a modular strategy to design synthetic fluorescent probes for live-cell nucleus imaging *Chem. Commun.* **50** 6149–52

[26] Lukinavičius G *et al* 2013 A near-infrared fluorophore for live-cell super-resolution microscopy of cellular proteins *Nat. Chem.* **5** 132–9

[27] Bucevičius J, Keller-Findeisen J, Gilat T, Hell S W and Lukinavičius G 2019 Rhodamine-Hoechst positional isomers for highly efficient staining of heterochromatin *Chem. Sci.* **10** 1962–70

[28] Sreedharan S *et al* 2017 Multimodal super-resolution optical microscopy using a transition-metal-based probe provides unprecedented capabilities for imaging both nuclear chromatin and mitochondria *J. Am. Chem. Soc.* **139** 15907–13

[29] Byrne A, Burke C S and Keyes T E 2016 Precision targeted ruthenium(ii) luminophores; highly effective probes for cell imaging by stimulated emission depletion (STED) microscopy *Chem. Sci.* **7** 6551–62

[30] Shen Y *et al* 2018 Visualization of mitochondrial DNA in living cells with super-resolution microscopy using thiophene-based terpyridine Zn(ii) complexes *Chem. Commun.* **54** 11288–91

[31] Heller I, Sitters G, Broekmans O D, Farge G, Menges C, Wende W, Hell S W, Peterman E J and Wuite G J 2013 STED nanoscopy combined with optical tweezers reveals protein dynamics on densely covered DNA *Nat. Methods* **10** 910–6

[32] Mitchell-Jordan S, Chen H, Franklin S, Stefani E, Bentolila L A and Vondriska T M 2012 Features of endogenous cardiomyocyte chromatin revealed by super-resolution STED microscopy *J. Mol. Cell. Cardiol.* **53** 552–8

[33] Swanson E C, Manning B, Zhang H and Lawrence J B 2013 Higher-order unfolding of satellite heterochromatin is a consistent and early event in cell senescence *J. Cell Biol.* **203** 929–42

[34] Swanson E C, Rapkin L M, Bazett-Jones D P and Lawrence J B 2015 Unfolding the story of chromatin organization in senescent cells *Nucleus* **6** 254–60

[35] Cseresnyes Z, Schwarz U and Green C M 2009 Analysis of replication factories in human cells by super-resolution light microscopy *BMC Cell Biol.* **10** 88

[36] D'Abrantes S, Gratton S, Reynolds P, Kriechbaumer V, McKenna J, Barnard S, Clarke D T and Botchway S W 2018 Super-resolution nanoscopy imaging applied to DNA double-strand breaks *Radiat. Res.* **189** 19–31

[37] Kukat C, Wurm C A, Spahr H, Falkenberg M, Larsson N G and Jakobs S 2011 Super-resolution microscopy reveals that mammalian mitochondrial nucleoids have a uniform size and frequently contain a single copy of mtDNA *Proc. Natl Acad. Sci. USA* **108** 13534–9

[38] Natale F *et al* 2017 Identification of the elementary structural units of the DNA damage response *Nat. Commun.* **8** 15760

[39] Kaniecki K, De Tullio L and Greene E C 2018 A change of view: homologous recombination at single-molecule resolution *Nat. Rev. Genet.* **19** 191–207

[40] Rogakou E P, Pilch D R, Orr A H, Ivanova V S and Bonner W M 1998 DNA double-stranded breaks induce histone H2AX phosphorylation on serine 139 *J. Biol. Chem.* **273** 5858–68

[41] Reindl J, Girst S, Walsh D W, Greubel C, Schwarz B, Siebenwirth C, Drexler G A, Friedl A A and Dollinger G 2017 Chromatin organization revealed by nanostructure of irradiation induced gammaH2AX, 53BP1 and Rad51 foci *Sci. Rep.* **7** 40616

[42] Reindl J, Drexler G A, Girst S, Greubel C, Siebenwirth C, Drexler S E, Dollinger G and Friedl A A 2015 Nanoscopic exclusion between Rad51 and 53BP1 after ion irradiation in human HeLa cells *Phys. Biol.* **12** 066005

[43] Anderson R *et al* 2019 Length-independent telomere damage drives post-mitotic cardiomyocyte senescence *EMBO J.* **38** e100492

[44] Gataulin D V, Carey J N, Li J, Shah P, Grubb J T and Bishop D K 2018 The ATPase activity of *E. coli* RecA prevents accumulation of toxic complexes formed by erroneous binding to undamaged double stranded DNA *Nucl. Acids Res.* **46** 9510–23

[45] Hernandez M R, Davis M B, Jiang J, Brouhard E A, Severson A F and Csankovszki G 2018 Condensin I protects meiotic cohesin from WAPL-1 mediated removal *PLoS Genet.* **14** e1007382

[46] Li Z, Fang C, Su Y, Liu H, Lang F, Li X, Chen G, Lu D and Zhou J 2016 Visualizing the replicating HSV-1 virus using STED super-resolution microscopy *Virol. J.* **13** 65

[47] Kukat C *et al* 2015 Cross-strand binding of TFAM to a single mtDNA molecule forms the mitochondrial nucleoid *Proc. Natl Acad. Sci. USA* **112** 11288–93

[48] Jezek P, Spacek T, Tauber J and Pavluch V 2019 Mitochondrial nucleoids: superresolution microscopy analysis *Int. J. Biochem. Cell Biol.* **106** 21–5

[49] Beater S, Holzmeister P, Lalkens B and Tinnefeld P 2015 Simple and aberration-free 4color-STED--multiplexing by transient binding *Opt. Express* **23** 8630–8

[50] Wang Y *et al* 2017 Rapid sequential *in situ* multiplexing with dna exchange imaging in neuronal cells and tissues *Nano Lett.* **17** 6131–9

[51] Schueder F, Strauss M T, Hoerl D, Schnitzbauer J, Schlichthaerle T, Strauss S, Yin P, Harz H, Leonhardt H and Jungmann R 2017 Universal super-resolution multiplexing by DNA exchange *Angew. Chem., Int. Ed. Engl.* **56** 4052–5

[52] Sharonov A and Hochstrasser R M 2006 Wide-field subdiffraction imaging by accumulated binding of diffusing probes *Proc. Natl Acad. Sci. USA* **103** 18911–6

[53] Jungmann R, Steinhauer C, Scheible M, Kuzyk A, Tinnefeld P and Simmel F C 2010 Single-molecule kinetics and super-resolution microscopy by fluorescence imaging of transient binding on DNA origami *Nano Lett.* **10** 4756–61

[54] Nieves D J, Gaus K and Baker M A B 2018 DNA-based super-resolution microscopy: DNA-PAINT *Genes* **9** 621

[55] Eilers Y, Ta H, Gwosch K C, Balzarotti F and Hell S W 2018 MINFLUX monitors rapid molecular jumps with superior spatiotemporal resolution *Proc. Natl Acad. Sci. USA* **115** 6117–22

[56] Balzarotti F, Eilers Y, Gwosch K C, Gynna A H, Westphal V, Stefani F D, Elf J and Hell S W 2017 Nanometer resolution imaging and tracking of fluorescent molecules with minimal photon fluxes *Science* **355** 606–12